Journal of Constructional Steel Research 234 (2025) 109723

Contents lists available at ScienceDirect

Journal of Constructional Steel Research

journal homepage: www.elsevier.com/locate/jcsr

Numerical and experimental reassessment of Eurocode 3 design rules for cellular beam end-posts

Georgios Psyrras [a], Konstantinos Daniel Tsavdaridis [a,*], R. Mark Lawson [a,b]

[a] Department of Engineering, School of Science & Technology, City St George's, University of London, Northampton Square, EC1V 0HB London, UK
[b] The Steel Construction Institute, Unit 2, The E Centre, Bracknell RG12 1NF, UK

ARTICLE INFO

Keywords:
Cellular beams
End-post
FE validation
Local buckling
Vierendeel mechanism
Notches and infill plates

ABSTRACT

This paper investigates the end-post behaviour of cellular beams focusing on the failure mechanisms subject to shear adjacent to the connections. Three cellular beams were tested to failure in a companion paper and their behaviours were modelled and validated herein using Abaqus. The cellular beams were connected to the columns through a bolted end-plate at one end and a bolted fin-plate at the other end. Finite element (FE) analyses were carried out for end-posts with and without notches, and web openings with half infill plates for cases where the minimum end-post width requirements were not satisfied. It was found that the FE results were in good agreement with the test results while both gave significantly higher failure loads than the design predictions provided by BS EN 1993-1-13. A parametric study was carried out on each connection side and in total 160 end-post models were examined. It was concluded that the connection type not only affected the end-post shear resistance but also influenced the failure mode. It was shown that using a half infill plate at the first opening can greatly increase the end-post's shear resistance.

1. Introduction

Cellular beams with large circular web openings have been widely used in long span steel and composite construction over 30 years. They are formed by cutting and re-welding rolled steel profiles to create deeper beams with multiple circular openings, or alternatively circular openings can be cut in the web of fabricated beams. The presence of large web openings introduces many potential failure mechanisms [1–5]. Publications including SCI P100 [6], SCI P355 [7], AISC Guides [8] and the recently published Eurocode 3 Part 1–13 [9] provide guidance on their design.

The *Vierendeel* mechanism, first reported by Altifillisch et al. [10] for castellated beams and later by Redwood and McCutcheon [11] for cellular beams, is associated with high shear forces that cause the formation of four 'plastic' hinges around the web opening. Redwood [12] and Ward [6] developed simplified analytical linear methods to estimate the *Vierendeel* bending action in cellular beams. To address the deficiencies of the analytical methods, Chung et al. [1,13] and Tsavdaridis and D'Mello [4] utilised non-linear FEA to develop shear/moment interaction design curves for the *Vierendeel* failure. More recently, with compute power increasing and the introduction of machine learning, studies that are analysing the combination of failure modes on full length cellular beams for ultimate load and design resistances have been developed [14,15].

Regarding the web-post behaviour, comprehensive research works involving both experimental and numerical testing have been presented by Tsavdaridis and D'Mello [3], Erdal and Saka [16], and Grilo et al. [17]. These studies have focused on web-post buckling behaviour between closely-spaced circular web openings, and on the prediction of the web-posts horizontal shear resistance. More recently, Shamass et al. [18], Ferreira et al. [19,20], Rabi et al. [21] and Santos et al. [22] have investigated the web-post buckling behaviour of steel and steel-concrete composite perforated beams with newer web opening shapes, such as the elliptically-based, a modification of the hexagonal shape used in the pioneering castellated beams of the 1960's.

The part of the web next to the connection at the ends of the beam is known as the 'end-post' but there is little guidance on their design, which is the subject of this paper. End-posts can be quite narrow, although the minimum width of an end-post next to a circular opening is taken as 0.25× opening diameter in Eurocode 3 Part 1–13 [9].

The failure modes of end-posts are affected also by the type of end connection to a column or a supporting beam. Often, it is necessary to

* Corresponding author.
E-mail address: Konstantinos.tsavdaridis@citystgeorges.ac.uk (K.D. Tsavdaridis).

https://doi.org/10.1016/j.jcsr.2025.109723
Received 15 April 2025; Received in revised form 23 May 2025; Accepted 7 June 2025
Available online 16 June 2025

introduce a half or full infill plate in the opening next to the connection to satisfy the dimensional limits and to achieve the required design shear resistance. Other strengthening techniques for cellular beams are the ring type stiffeners [23].

Cellular beams may also be manufactured as asymmetric sections using two different rolled sections. The shear forces may be assumed to be transferred by the Tees in proportion to their shear area. In such cases, the shear force resisted by top Tee is generally critical as this can lead to buckling of the end-post [24].

The possible modes of failure of the end-posts, which are presented in Appendix A, are:

- Horizontal shear failure at its narrowest width at the centre-line of the openings.
- End-post buckling as a strut due to the compression force transferred from the top Tee.
- In-plane bending failure of the narrow end-post due to horizontal shear.
- Local high stress effects at notches to the flange and web at beam-to-beam connections (known as a 'notched beam').

Two generic connection types are considered in this study:

- Bolted connections to the beam web either by fin-plates or angles.
- Welded end-plate connections in which the end-plate is either connected only to the beam web (partial depth end-plate) or also to the flanges (full depth end-plate).

For end-plate connections, the end-plate can strengthen the end-post in horizontal shear and bending, and also partly stabilises the web against buckling. Conversely, bolted fin-plate or angle connections lead to a reduction in the shear and bending resistance at the line of the bolt holes and may provide less restraint to end-post buckling.

A half infill (semi-circular) plate of approximately the same thickness as the web may be welded to the edge of the opening next to the end-post to increase its width and shear resistance. In this case, buckling of the infill plate may be the critical mode of failure.

Notches of the beam flanges may be required at beam-to-beam connections. Notches cause increased stress concentration in the narrow web between the notch and the opening. The rules for the maximum size of notches in SCI publication 'Joints in Steel Construction' [25] were developed for solid web beams which give a maximum notch depth of 0.1 h and a maximum notch length of 0.2 h, where h is the beam depth.

Research on the end-post behaviour next to connections is limited. When the end-post width, s_e, fulfils $s_e \geq 0.5s_o$, where s_o is the width of the adjacent web-post, it was previously assumed that the end-post is not as critical as the first web-post, but this may not be the case because of the different conditions at the connections. The design method for end-posts given in [9] is based on a modification to the web-post buckling method, which is known to be conservative.

Tsavdaridis et al. [26] investigated whether the design approach in [9] could be verified based on a series of tests on cellular beam-to-column connections.

The objectives of the paper are therefore:

- To model the tests on end-posts to cellular beams and their connections using Abaqus in order to verify the test results in terms of the failure load and the load-deflection curve.
- Having verified the tests, to extend the range of design cases using the same modelling method to include openings with a range of diameters, end-post widths and flange notch lengths.
- To present a relatively simple theory on the various failure modes for the end-posts as influenced by the connections and half infill plates to the openings and to compare the finite element results to the design predictions.

2. Cellular beam tests on end-posts with 2 connection types

The beam tests reported by Tsavdaridis et al. [26] used 406x178x67kg/m UB sections in S355 steel to form cellular beams of depth h = 559 mm with opening diameters, $h_o = 400$ mm ($h_o = 0.71$ h). Three 3.62 m long beams shown in Fig. 1 were tested with practical end-post configurations, as follows:

1. Beam with narrow end-post of 90 mm width ($s_e = 0.225h_o$).
2. Beam with 90 mm wide end-post and 90 mm wide x 60 mm deep notches with a 20 mm radius corner to the flanges.
3. Beam with notched flanges (as in '2') with a 200 mm wide half infill plate of 8 mm nominal thickness, forming an end-post of 203 mm width ($s_e = 0.51$ h_o).

The beams were cut from one longer piece for consistency of their properties. Each beam had a fin-plate connection on one side and an end-plate connection on the other to enable their direct comparison. Two connection types were tested:

- End-plate connection using a 12 mm thick end-plate with 2 × 4 no. M20 bolts to the column flange.
- Fin-plate connection using a 12 mm thick projecting welded plate of 440 mm depth with 5 no M20 bolts to the beam web.

The beam specimens were connected with columns using 203x203x60 UC sections of 1 m height. Two jacks were positioned at 803 mm from either end of the beam and applied the incremental load to the beams. Web stiffeners and full infill plates were used at those locations and the beams were laterally restrained at mid-span. The two jacks were loaded simultaneously; the first failure occurred at fin-plate side, and then the jack load on this side was monitored as the jack load on the end-plate side was increased to failure.

Table 1 summarises the test failure loads and their modes. The results showed that the end-post at the end-plate connection failed at 2 to 7 % higher load than at the fin-plate side. The presence of notches reduced the shear resistance of the narrow end-posts, causing the beams to fail by buckling in the notch region at 8 to 13 % lower shear force than the corresponding un-notched beam. The half infills increased the failure loads of the notched beam by 40 to 43 % for the same connection type and buckling of the infill plates occurred in a similar manner for both the end-plate and fin-plate connections. The test failure loads were compared to the end-post buckling resistances given in the Eurocode 3 Part 1–13 [9] and exceeded the predicted resistances by 49 % to 73 %, which shows that the Eurocode method is conservative, particularly for the full depth end-plate connections.

The reason for the Eurocode model being conservative is that it was developed 5 years before the tests by Tsavdaridis et al. [26] and therefore had to be demonstrably 'on the safe side' using an extension of the web-post buckling rules that had been calibrated extensively in order to prepare design rules. Also, the conditions in the end-post depend on the type of connection and the boundary conditions that differ from the web-post.

3. FE modelling of cellular beam tests

3.1. Modelling and analysis of the tests

The cellular beam tests were modelled and analysed using Abaqus [27]. The loads were applied directly to the beams over the area of the load cells. The column base-plate restraints and the lateral torsional buckling restraints were not modelled, instead boundary conditions were applied directly to the base of the columns and to the beam flanges, respectively. At the base-plate restraints, some minor differences were expected to affect the beam behaviour. In the test set-up, the column bases were welded to the base-plates that were partially restrained by

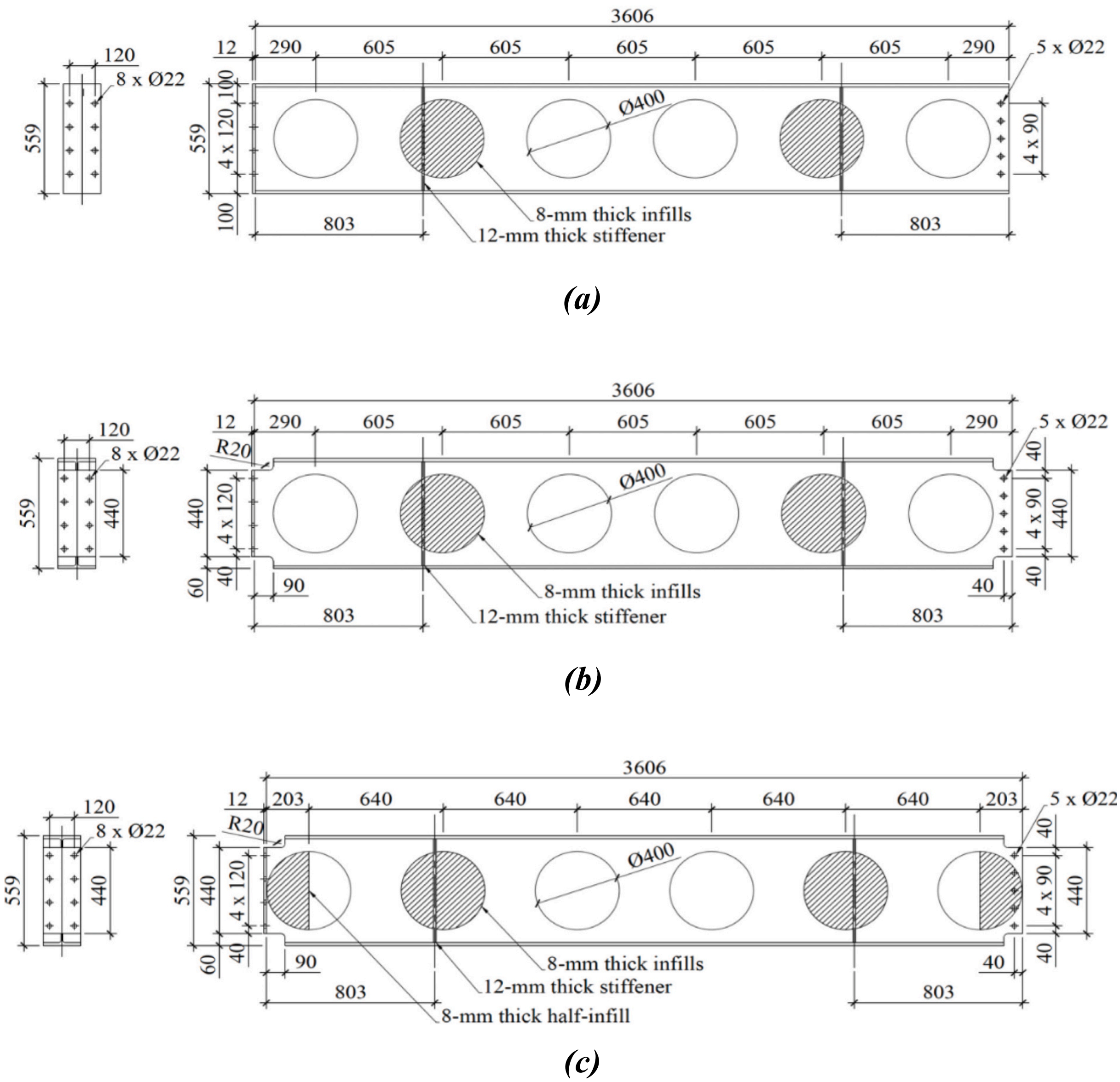

Fig. 1. Details of cellular beams in the tests: (a) narrow end-post, (b) narrow end-post with notches, (c) half infill plate end-posts with notches (Tsavdaridis et al. [26]).

Table 1
Test shear failure loads of end-posts and comparison with the design predictions to BS EN 1993-1-13 [9] using measured properties.

Test beam with	Connection type	Shear failure load	BS EN 1993-1-13 calculation	Failure mode in test
90 mm wide end-post	Fin-plate	325 kN	188 kN	End-post bending
	Full depth end-plate	331 kN	197 kN	*Vierendeel* bending at full opening
90 mm wide end-post with 90 mm × 60 mm notches	Fin-plate	279 kN	178 kN	Buckling at notch
	Partial depth end-plate	298 kN	193 kN	Lateral movement of flange at notch
Half infill plate (200 mm wide) with 90 mm × 60 mm notches	Fin-plate Partial depth end-plate	398 kN 417 kN	263 kN 279 kN	Buckling of half infill plate

horizontally placed PFC beams, allowing some uplift of the columns. This uplift might allow the columns to lean inwards during the loading, leading to slightly higher mid-span deformation of the beams. However, in the FE models, the column bases are assumed as pinned. All tests were modelled as 3D planar shell parts, as shown in Fig. 2.

3.1.1. *Material properties*

A bilinear stress-strain curve was used to model the steel material behaviours. The values of the steel yield strength, f_y, and ultimate strength, f_u, were provided through mill test certificates by the supplier, and are given in Table 2. The beam stiffeners, the end-plates and the fin-plates were all modelled using their material properties.

3.1.2. *FE meshing*

To accurately mesh the three models a combination of 4-node reduced integration shell elements (S4R) and 3-node reduced integration shell elements (S3) was employed. Finite membrane strains and second order accuracy were also enabled for both shell element types throughout the analysis. A mesh convergence study was conducted to choose the approximate mesh global element size. Four mesh sizes were

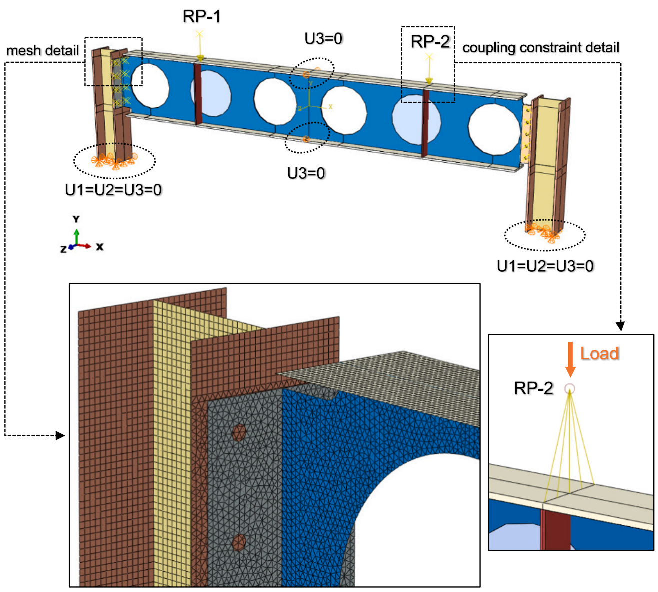

Fig. 2. Finite element modelling of Test 2. Identical boundary conditions and loads were applied to all models.

Table 2
Material and dimensional properties of steel specimens (E = 200 GPa and v = 0.3 for steel).

	Web thickness	Flange thickness	f_y	f_u	ε_u
Beams	9.0 mm	14.3 mm	393 MPa	470 MPa	0.20
Columns	9.4 mm	14.2 mm	398 MPa	550 MPa	0.20
Infill Plates	7.8 mm	–	469 MPa	600 MPa	0.20

examined by comparing the applied load against mid-span deflection curve to the respective test curve. Densely meshed models with element edges of approximately 7.5 mm (Fig. 2) captured the test behaviours adequately, and were selected for the further analyses.

3.1.3. *Interaction properties*

Node-to-surface 'Tie' constraints tying all degrees of freedom (DOFs) were used to model the welds between the fin-plates and the columns, as well as between the end-plates and the cellular beams. Bolted connections were modelled by using rigid beam constraints, ensuring that there would be no failure in the M20 bolts (no bolt failure occurred in the tests). In addition, this type of constraint prevented penetration between adjacent planar surfaces that would result in unrealistic model behaviours. Kinematic coupling constraints were used to model the lab tests' jacks (Fig. 2). A reference point (RP) was created for each load and was set as the control point. In this way, the applied loads were uniformly distributed across the width of the beam top flange.

3.1.4. *Boundary conditions and loads*

As part of the modelling simplifications, all translational DOFs (U1 = U2 = U3 = 0) at the column bases were constrained, essentially making both supports act as fixed. In addition, the beam flanges at the mid-span of the beam were restrained laterally (U3 = 0), to model the lateral buckling restraint in the test (Fig. 2). Two concentrated loads were applied, one at each reference point. The values of the concentrated loads varied depending on the type of the analysis.

3.1.5. *Analyses steps*

The following loading protocol was implemented to obtain two test results for each beam and to be able to directly compare the modes of failure for the end-posts to the two connection types:

1. Load both jacks to 40 kN and un-load to allow for slip of the bolts into bearing.
2. Load both jacks up to 200 kN and un-load to 40 kN.
3. Load both jacks until the first failure on the fin-plate connection side.
4. Unload both jacks to 200 kN.
5. Load the jack closer to the end-plate side, whilst recording the load in the load cell on the fin-plate side, which reduces with increasing displacement of the beam. From the recorded load in the two load cells, the shear force in the end-plate connection is determined up to the failure point.
6. Unload to determine the residual displacements due to deformation of the end-posts.

The analyses of all beams showed that the first two loading and unloading steps did not affect the outcome of the analyses, and they could be ignored in the FEA. However, in the tests, these two steps were necessary in order to ensure the bolts went into bear and to minimise slip in the subsequent loading steps. More details on the loading protocol can be found in [26].

Two different types of analyses were carried out for this study:

- Geometrically and materially nonlinear static analyses with imperfections (GMNIA) using the Riks method of the Abaqus Standard Solver, which can predict the response of the specimen until the first beam failure (step 3).
- Pseudo-static analyses using the Abaqus Explicit Solver, which can simulate the whole loading test procedure including the second beam failure (steps 3–5).

The Riks method successfully modelled the first test for all three specimens, i.e. until the first failure occurs (step 3), but was unable to model the subsequent loading until the second failure occurred (steps 3 to 5), as a Riks step cannot be followed by another step in the same analysis [28], and hence the second loading stage on each specimen had to be modelled in a different way. Another approach is to consider mass inertia in the modelling and treat the buckling response dynamically. Abaqus Explicit Solver can handle post-buckling problems and allows modelling of both loading tests in a single analysis. In this case the loads are applied slowly, in a 'quasi-static' way, to prevent dynamic effects from dominating the solution. The computational cost of this analysis is significantly greater than with the Static Riks method.

3.1.6. *Finite element (FE) results*

When FE results are compared to the beam test results, it was observed that the differences between the Explicit Solver and the Standard Solver model analyses were minor. Both solutions gave similar load-displacement curves and agreed on the first beam failure mode and load. Since the Riks analysis (Standard Solver) could not be used to model the full loading procedure, only the Explicit Solver analyses are discussed in the following sub-sections.

3.1.6.1. Narrow end-post (Test 1). The load-displacement curves for this test with narrow end-posts but without notches are shown in Fig. 3. The vertical axis represents the shear force at both ends of the beam plotted against the mid-span vertical displacement (U2) measured at the bottom of the beam at mid-span.

It was evident from the test curves that there was some bolt slippage during the initial loading and unloading. This was indicated by the different stiffness slopes during loading steps 1–3 between test and FE results, while the beam behaviour was elastic. The actual stiffness of the tested frame, after the bolts went fully into bearing, is the slope of the black dashed line, which agrees with the elastic responses of both FE models. In the FE analyses, a linear behaviour was recorded up to a shear force of 233 kN, which was at 74 % of the failure load (313kN) of the fin-plate side, compared to the failure load of 321 kN in the test. This was

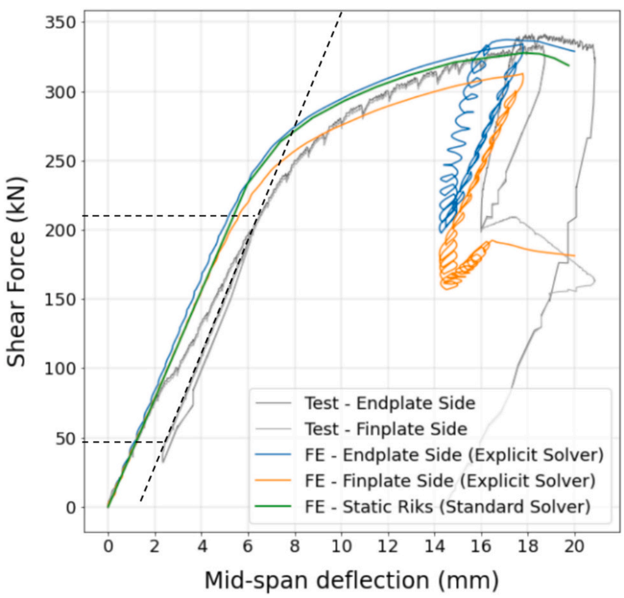

Fig. 3. Shear force vs. Mid-span vertical deflection curve (Test 1).

attributed to the local buckling of the edge of the web opening, as shown in Fig. 4 due to the high vertical stresses acting on it. The FE mid-span deflection at the predicted failure load was 17.8 mm, only 0.9 mm less than in the test. The maximum compression stress given in Fig. 4c was 465 N/mm^2 which is close to the ultimate steel strength and shows that high local strains had developed. Locally high stresses are apparent in the end-post next to the top and bottom bolts.

The second failure occurred on the end-plate connection side at a shear load of 331 kN, similar to 325 kN recorded in the test. This failure occurred at a mid-span deflection of 16.2 mm, which was 2.1 mm less than in the test. The failure mode occurred by the formation of ‘plastic’ hinges due to the high *Vierendeel* bending moments at the first opening next to the end-plate connection as shown in Fig. 5a.

Fig. 5b shows the maximum in-plane principal stresses at the failure load. Locally, the maximum compression stress exceeded the ultimate strength of the steel which shows that high plastic strains had developed (Fig. 5c) at the angles of approximately 30^o to the vertical around the opening. This is consistent with the *Vierendeel* bending failure mode, which is independent of the end-post.

3.1.6.2. Notched beam with narrow end-post (Test 2). The model analyses for the notched beam with 90 mm wide end-posts results agree well with the test results. The load - displacement curves are presented in Fig. 6.

In the FE model, the failure occurred on the fin-plate connection side by buckling of the narrow web at a shear force of 277 kN, which is close to the test failure load of 279 kN. In this case, the model behaviour was linear up to 80 % of the failure shear force at the fin-plate side.

The stresses across the minimum width of the web at the notch are shown in Fig. 7c. Although the main upper part of the web near the opening is in compression, the web near the notch is in tension, indicating that the narrow web at the notch is subject to in-plane bending. The high compressive stresses at the top Tee near the notch (Fig. 7b and c) caused the buckling of the narrow web, which was the observed failure mode. Furthermore, out-of-plane movement of the top flange was observed in the model, as the upper Tee was partially unrestrained due to the notch. Increased stress concentrations were also observed around the second bolt from the top of the 5-bolt connection (Fig. 7c).

Then the load on the end-plate side jack was increased until failure in the FE model at a shear force of 288 kN, which was 3.4 % less than the test failure load of 298 kN. The end-plate connection side failed by local buckling due to the high compressive stresses in the narrow web close to the notch. Redistribution of stresses between the top and bottom Tees occurred when buckling became more pronounced. In addition, there was significant lateral movement of the top flange relative to the end-plate, which was also observed in the test.

For the end-plate connection, the maximum in-plane principal stresses at failure in Fig. 8c show that the narrow part of the web at the notch was fully in compression without in-plane bending, while the corner of the bottom notch showed some in-plane bending. The unequal

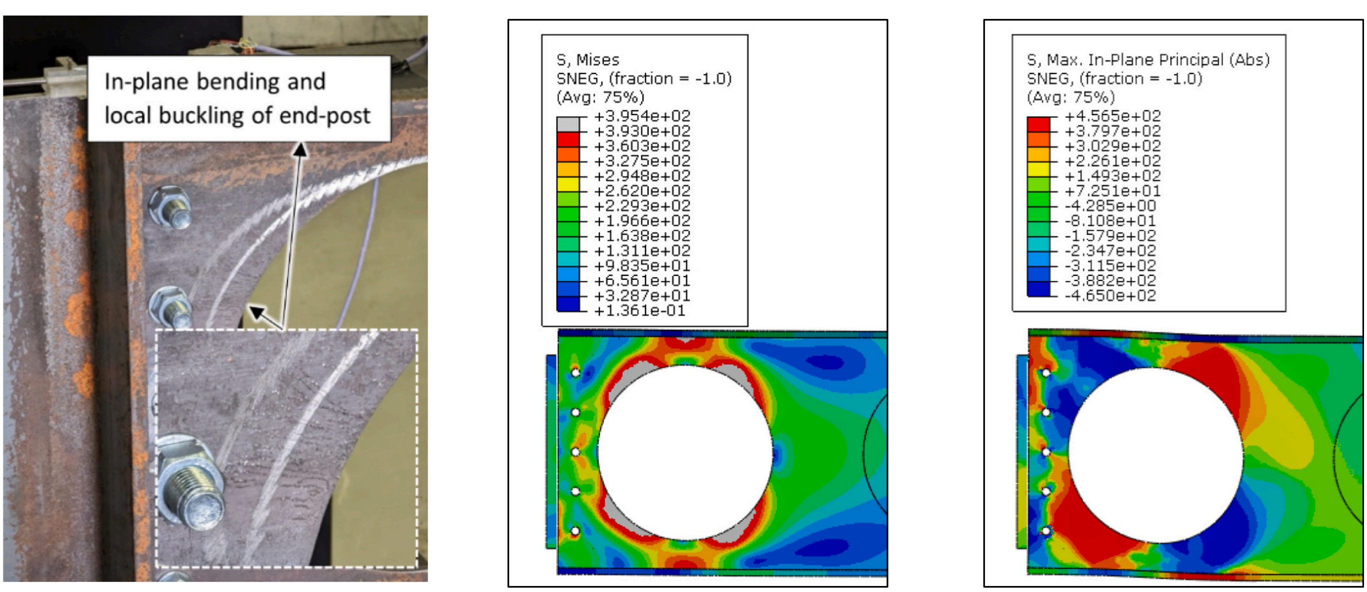

***(a)** Failure on the fin-plate connection side during test (Tsavdaridis et al.[26])*

***(b)** Von Mises stresses (MPa) at the yield limit (233 kN)*

***(c)** Max. absolute in-plane principal stresses (MPa) at failure (313 kN)*

Fig. 4. First failure at the shear force of 313 kN on the fin-plate connection side (Test 1).

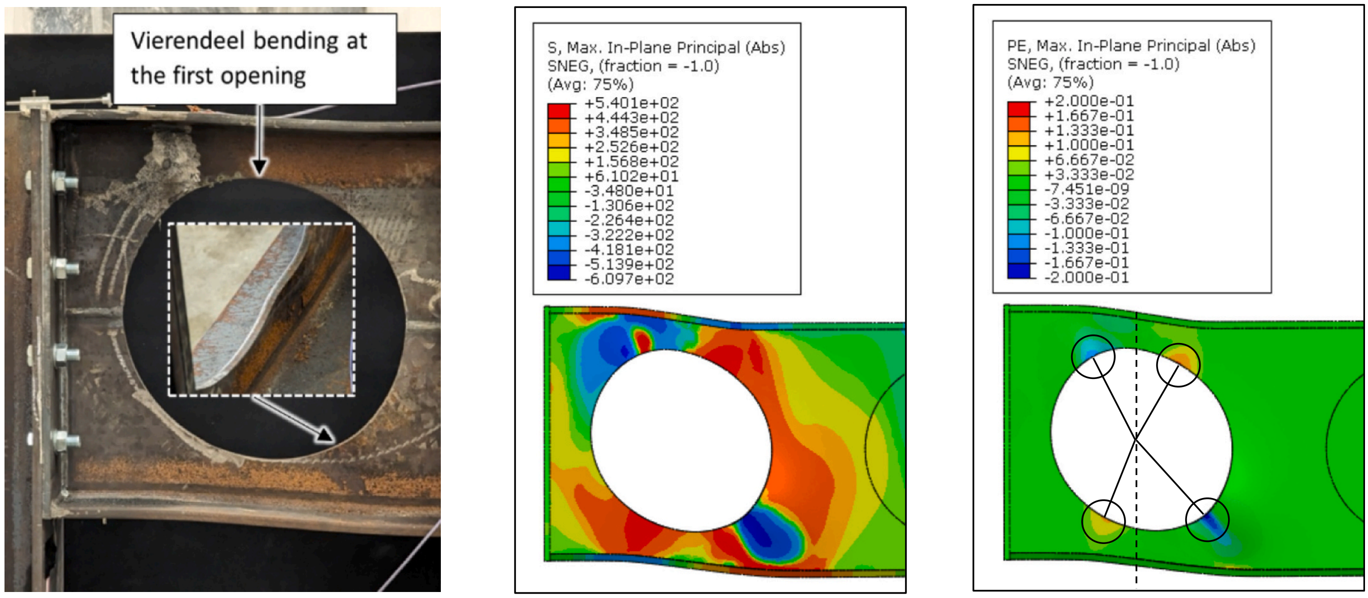

***(a)** Failure on the end-plate connection side during test (Tsavdaridis et al. [26])*

***(b)** Max. absolute in-plane principal stresses (MPa) at failure (331 kN)*

***(c)** Max. principal strains (MPa) at failure (331 kN)*

Fig. 5. Second failure at the shear force of 331 kN on the end-plate connection side (Test 1).

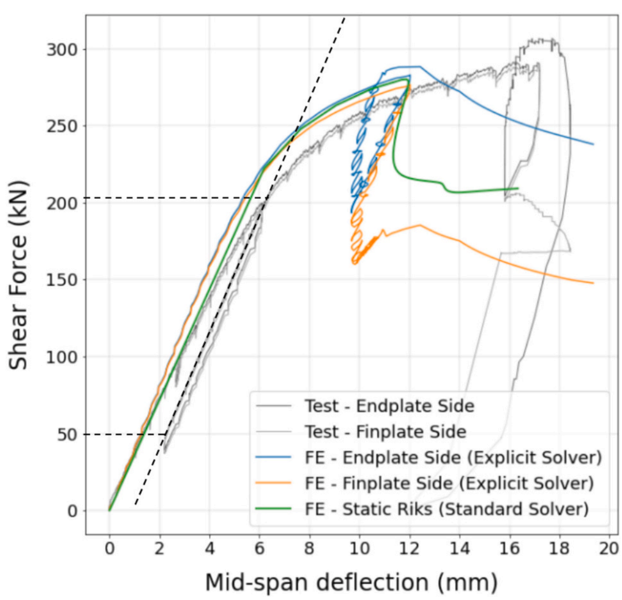

Fig. 6. Shear force vs. Mid-span vertical deflection curve (Test 2).

stress distribution in the top and bottom Tees also indicated some redistribution of forces to the bottom Tee.

3.1.6.3. Notched beam with half infill plate (Test 3). The load - displacement curves for the test with half infill plate at the first opening are shown in Fig. 9. It is clear that during the test an additional displacement occurred as the bolts slipped into bearing, in a similar way to Test 1, which is indicated by the significant variations in the slope of the curves while the frame behaviour was still elastic. The correct frame stiffness was developed after the bolts were in bearing, which occurred during loading step 3 - highlighted with the black dashed line in Fig. 9.

Both test and FE model showed elastic behaviour up to a shear force of 282 kN (67 % of the failure load). In the model analysis, failure on the fin-plate side occurred at a shear force of 417 kN (5 % higher than the test failure load of 398 kN). The mid-span vertical displacement at the failure load in the FEA was 15.8 mm, similar to the 16.2 mm in the test. The model failed by buckling of the half infill plate caused by the high compressive stresses at the top of the infill plate. At the failure load, redistribution of stresses from the upper Tee in compression towards the bottom Tee in tension had developed (Fig. 10c).

The model analysis continued, and the failure occurred on the end-plate side at a shear force of 431 kN, which was 3.4 % higher than the 417 kN failure load in the test. The end-plate connection side failed by *Vierendeel* bending of the half-opening, with some transverse movement of the top flange). The principal stresses shown in Fig. 11c are similar to those of the fin-plate side.

It should be noted that the plastic hinges are not easily observed in such cases; two hinges were formed early at the corners of the half opening, while further hinges started to appear on the edge of the semi-circle. Unlike the test, buckling of the infill plate was not observed in the FE model, probably because the welds to the infill plate in the test did not provide full continuity that was assumed in the FE model.

3.1.7. Summary of the validation findings

The following concluding observations are made from the FE analyses:

- The FEA results are in good agreement with the test results, validating the failure mechanisms and load resistances of the tests. It is reasonable to assume that the test setup and modelling assumptions were accurate. The two Abaqus solvers, Standard and Explicit, gave similar results. However, Standard solver provides a computationally more efficient solution, thus it may be used for the subsequent study on the failure of the end-posts at cellular beam connections.

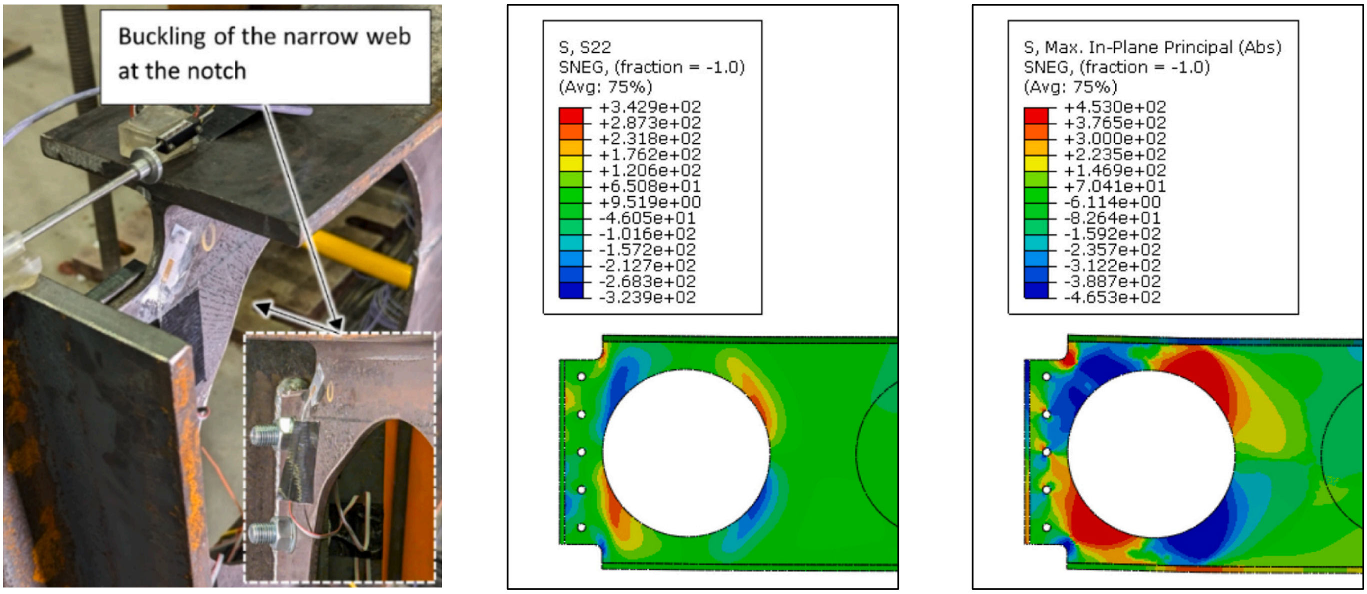

(a) *Failure on the fin-plate connection side during test (Tsavdaridis et al. [26])*

(b) *Vertical stresses S22 (MPa) at the yield limit (222 kN)*

(c) *Max. absolute in-plane principal stresses (MPa) at failure (277 kN)*

Fig. 7. First failure at the shear force of 277 kN on the fin-plate connection side (Test 2).

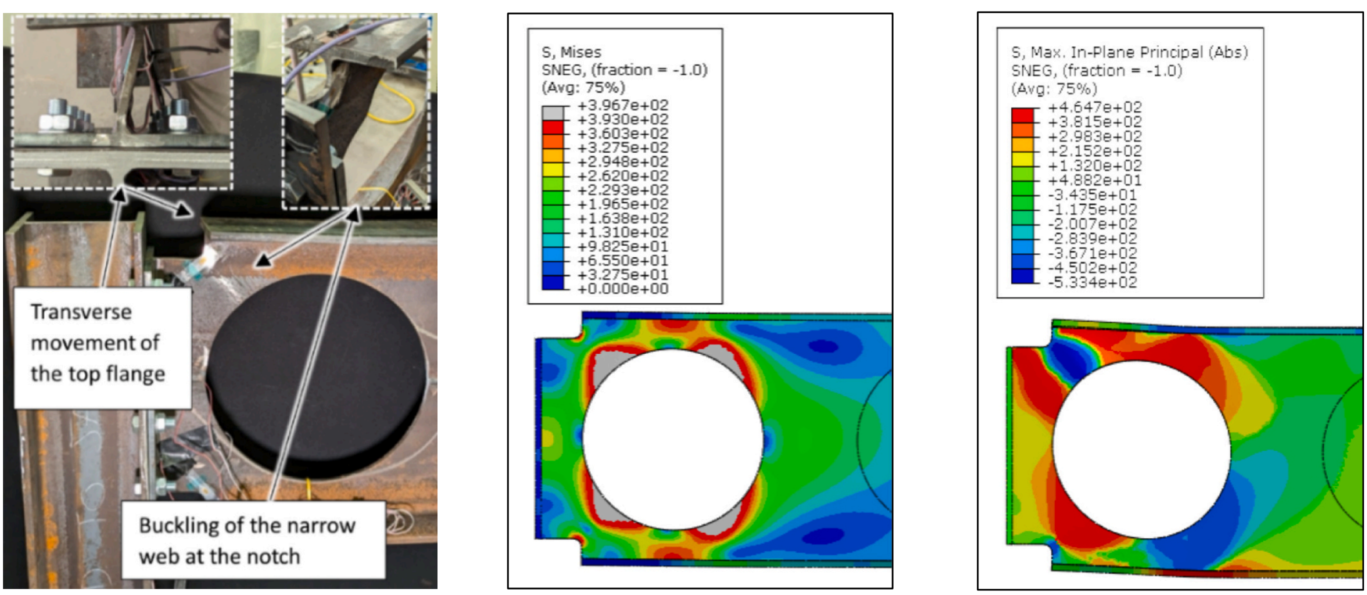

(a) *Failure on the end-plate connection side during test (Tsavdaridis et al. [26])*

(b) *Von Mises stresses (MPa) at the* yield *limit (222 kN)*

(c) *Max. absolute in-plane principal stresses (MPa) at failure (288 kN)*

Fig. 8. Second failure at the shear force of 288 kN on the end-plate connection side (Test 2).

- All three FE models confirm that the end-posts with end-plate connections are stronger than the end-posts with fin-plate connections, which is in line with the previous tests.
- The presence of notches reduces the shear resistance of the end-posts. The effect of notches was to reduce the end-post shear resistance by 11.5 % at the fin-plate side and by 13.6 % at the end-plate side. Both notched beam models exhibited high stress concentrations locally at the notches and it was seen that local bending effects occurred in the reduced web depth in the narrow end-post region.

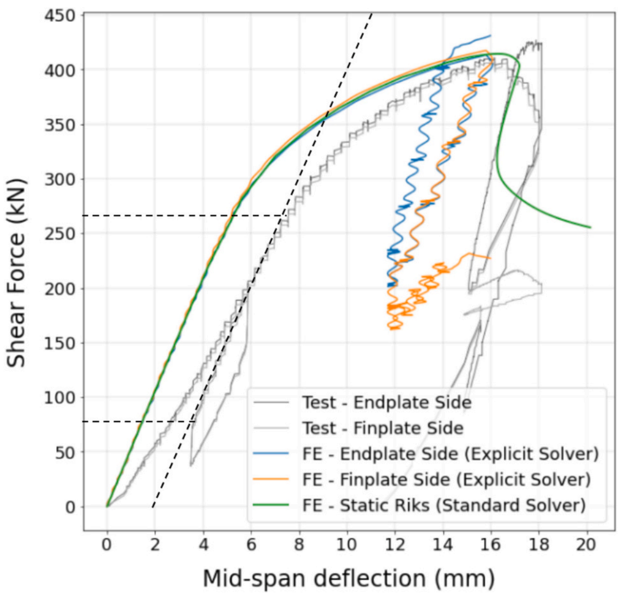

Fig. 9. Shear force vs. Mid-span vertical deflection curve (Test 3).

- Both beams with the notches (Tests 2 and 3) exhibited local instabilities in all their failures, as out-of-plane lateral movement of the upper flange was observed, caused by the lack of local restraint at the notches.

4. Parametric study

To extend and further validate the previous study, the shear resistance of the end-posts for the two types of connection side was analysed separately but using the same beam geometry and steel properties as for the tests. The key fixed parameters are the beam height, h = 559 mm, web thickness, $t_w = 9$ mm and measured steel strengths given in Table 1. For the cases with half infills, the plate was 7.8 mm thick and the end-post length was 203 mm as in the test, independent of the opening diameter. A further model of the half infill plate without notches was also analysed to compare with Test 3 which had notches.

4.1. Modelling assumptions

Identical modelling assumptions were made for all test specimens. The full models were set up as half span beams allowing for symmetry about mid-span. Although the original full test set-up was not purely symmetric due to the different connections on either side, it is reasonable to ignore the small difference in the connection stiffnesses and model the isolated connection sides using axisymmetric boundary conditions, as shown in Fig. 12. The other boundary conditions and interactions were adopted from the full test models, including the lateral restraints at mid-span.

Regarding the loading and analysis steps, load was applied to the beam over the stiffener until the first failure occurred, which is achieved through a GMNIA using the Abaqus Standard Solver's Buckling and Static Riks analyses.

4.2. Validation of isolated models

All isolated models were compared against the full models described earlier. The results showed that the analyses of the isolated models presented similar behaviour to the full models. The good agreement also further validated the test results. The load - displacement curves (Fig. 13) show that the isolated models and full models had similar stiffness, while the differences in the failure loads were less than 5 %.

4.3. Parametric study

A range of end-post geometric configurations were examined for

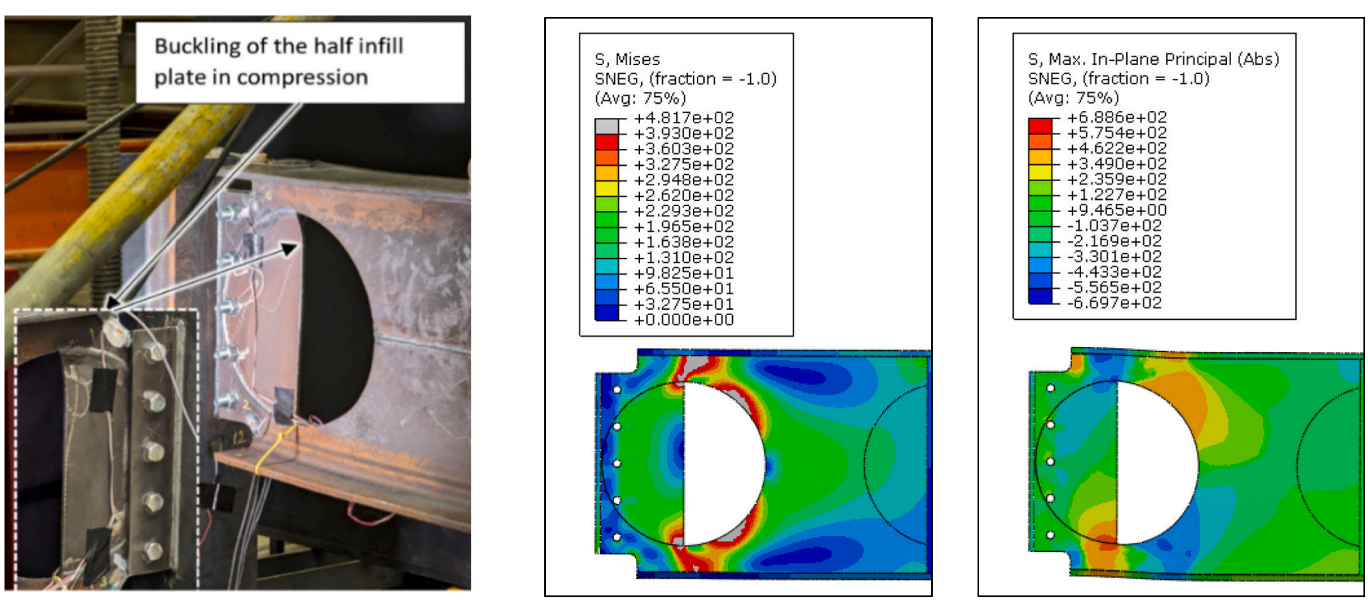

(a) *Failure on the fin-plate connection side during test (Tsavdaridis et al. [26])* ***(b)*** *Von Mises stresses (MPa) at the yield limit (282 kN)* ***(c)*** *Max. absolute in-plane principal stresses (MPa) at failure (417 kN)*

Fig. 10. First failure at a shear force of 417 kN on the fin-plate connection side (Test 3).

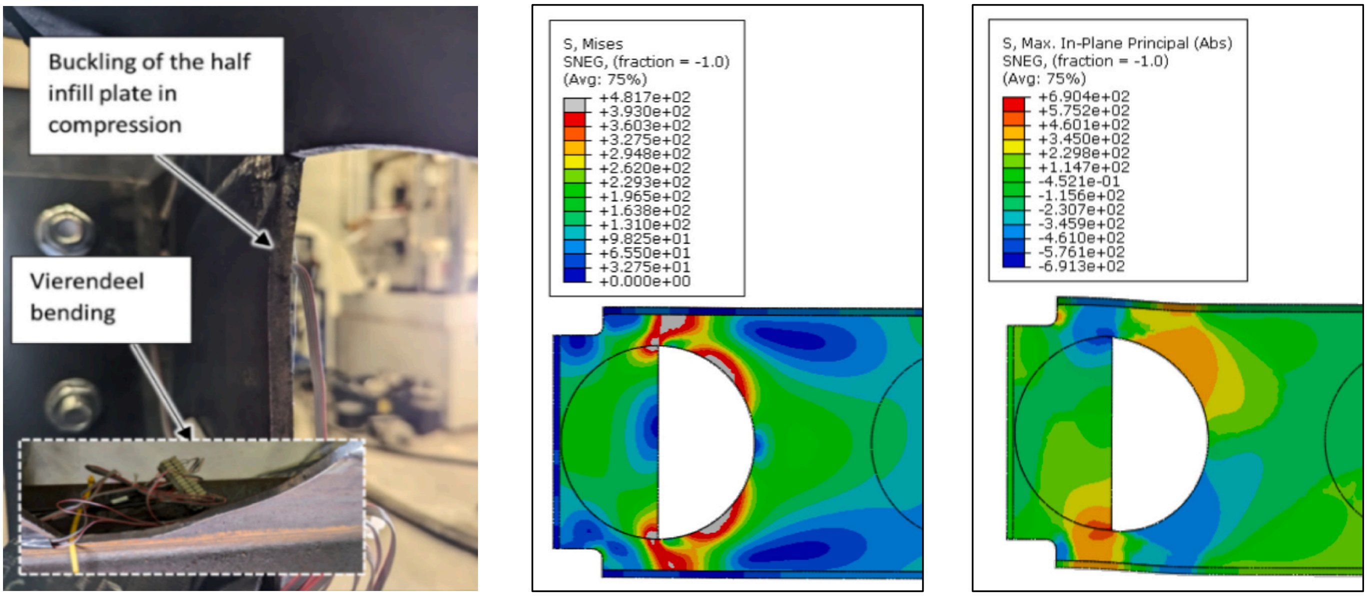

***(a)** Failure on the end-plate connection side during test (Tsavdaridis et al. [26])*

***(b)** Von Mises stresses (MPa) at the yield limit (282 kN)*

***(c)** Max. absolute in-plane principal stresses (MPa) at failure (431 kN)*

Fig. 11. Second failure at a shear force of 431 kN on the end-plate connection side (Test 3).

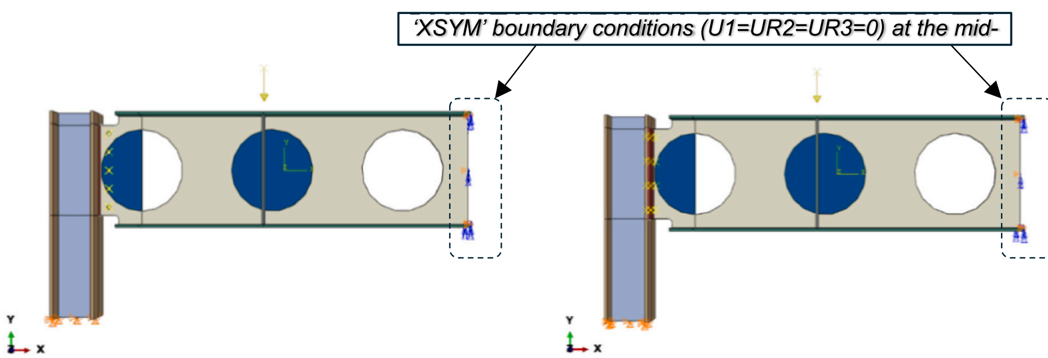

***(a)** Fin-plate connection side.*

***(b)** End-plate connection side.*

Fig. 12. Isolated models for Case 3.

each of the cases in Table 3. These configurations varied depending on the opening diameter (h_o), the end-post width (s_e) and the notch length (c_n). In total, 160 cases were analysed, including both end-post connection types. The following naming convention is used to refer to a specific modelling case. The cases with half infills had the same data as used in the tests, in which the end-post width was 203 mm and the infill plate was 7.8 mm thick (Table 3).

4.4. Analysis of case 1 models with narrow end-post

The results of the analyses for Case 1 of narrow end-posts with the two connection types are given in Table 4, compared to the theory presented in this paper. In this case, the practical range of opening diameters, h_o was 350 mm to 425 mm, and the end-post width s_e was 90 mm to 130 mm.

All models of the end-plate side of the narrow end-post without notches failed by *Vierendeel* bending, as was observed in the beam test, and so the parameter, s_e, did not affect the end-post resistance, except for the opening with $h_o = 350$ mm (Fig. 14a). In these cases, the possible theoretical failure modes are Modes 1, 2 and 3b (see Appendix A), and the theoretical failure load was taken as the smallest of those.

The majority of the fin-plate side models failed by the buckling of the narrow end-post. However, in the cases of 425 mm opening diameter and end-post width, $s_e \geq 100$ mm, failure occurred by *Vierendeel* bending. The theoretical failure loads are in all cases governed by end-post buckling (Mode 2), and it is relatively conservative, although the accuracy improves for deeper openings with wide end-posts. It should also be noted that the FE models allow very high strains and redistribution of forces between the top and bottom Tees, which is not included in the design model.

For the two connection types, the end-plate provided more stability to the end-post and increased the end-post failure load by 5.3 % on average compared to the fin-plate (see Table 7), but the larger the opening diameter, the less effect the connection type had on the end-post resistance.

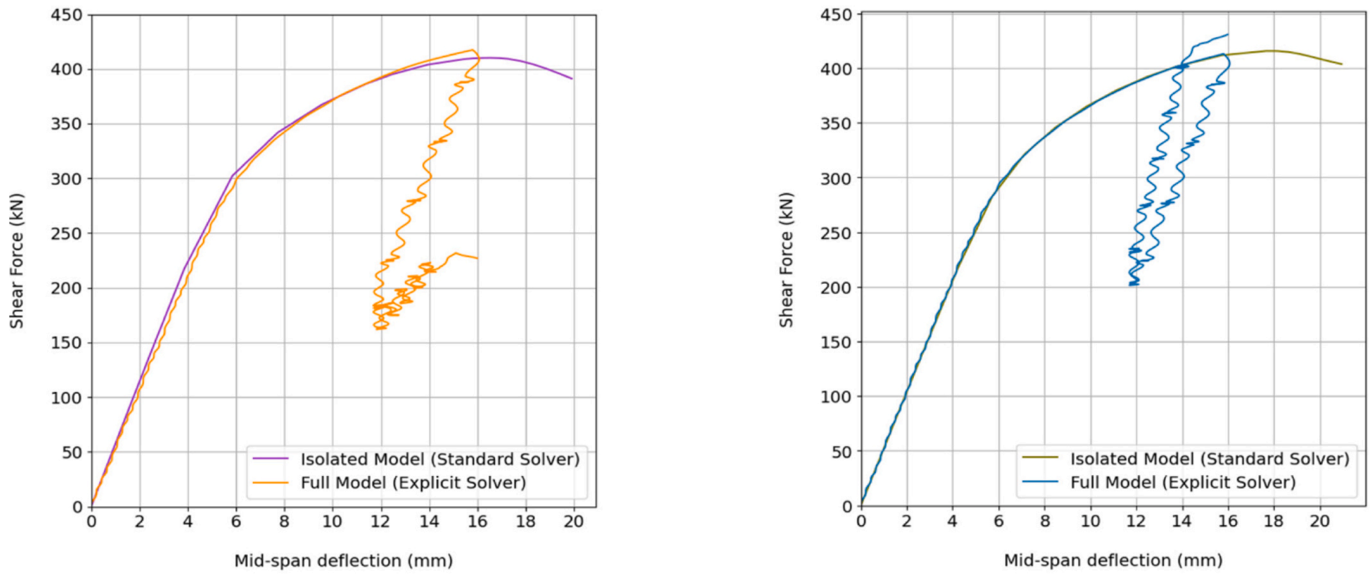

***(a)** Fin-plate side (Test 3)* ***(b)** End-plate side (Test 3)*

Fig. 13. Shear force vs. mid-span vertical displacement curves for the models for beams with half infill plates next to the connections (Test 3).

Table 3
Examined cases in the parametric study of end-post geometry.

		Parameters												
		Opening diameter h_o (mm)				End-post width s_e (mm)					Notch length c_n (mm)			
		350	375	400	425	90	100	110	120	130	90	105	120	135
Models	Case 1	✓	✓	✓	✓	✓	✓	✓	✓	✓	–	–	–	–
	Case 2	✓	✓	✓	✓	✓	✓	✓	✓	✓	✓	✓	✓	✓
	Case 3	✓	✓	✓	✓	–	–	–	–	–	✓	✓	✓	✓
	Case 4	✓	✓	✓	✓	–	–	–	–	–	–	–	–	–

Table 4
Parametric study results compared to the theory in this paper for narrow end-posts. VB is the failure load due to *Vierendeel* bending at the first opening, indicating that end-post failure did not occur.

Opening Diameter	End-post width, s_e (mm)	Fin-plate connection			End-plate connection		
		FE failure load (kN)	Theory (kN)	FE/Theory	FE failure load (kN)	Theory (kN)	FE/Theory
350 mm (=0.62 h)	90	388	222	1.75	422 VB	226	1.86
	100	397	246	1.61	431 VB	250	1.72
	110	401	267	1.50	434 VB	276	1.57
	120	409	288	1.42	435 VB	296	1.47
	130	413	312	1.32	437 VB	321	1.36
375 mm (=0.67 h)	90	349	197	1.77	386 VB	208	1.85
	100	358	218	1.64	389 VB	232	1.67
	110	366	236	1.55	386 VB	254	1.52
	120	370	254	1.45	386 VB	266	1.45
	130	374	275	1.36	386 VB	300	1.98
400 mm (=0.71 h)	90	312	193	1.61	338 VB	199	1.69
	100	322	211	1.53	337 VB	221	1.53
	110	329	232	1.42	338 VB	226	1.49
	120	329	253	1.30	338 VB	257	1.31
	130	328	269	1.22	337 VB	279	1.21
425 mm (=0.76 h)	90	278	182	1.53	287 VB	180	1.59
	100	282 VB	203	1.39	288 VB	200	1.44
	110	283 VB	220	1.29	287 VB	217	1.32
	120	283 VB	240	1.18	286 VB	232	1.22
	130	284 VB	260	1.09	287 VB	251	1.14

4.5. Analysis of case 2 models with narrow end-post and notches

The results of the analyses for Case 2 models with narrow end-posts, end notches and with the two connection types are given in Table 5. In this case, and the notch length c_n was 90 mm to 135 mm. Only the cases with the end-post width exceeding the notch length ($s_e \geq c_n$) were considered.

All 80 examined cases for end-posts with notches in beams failed by

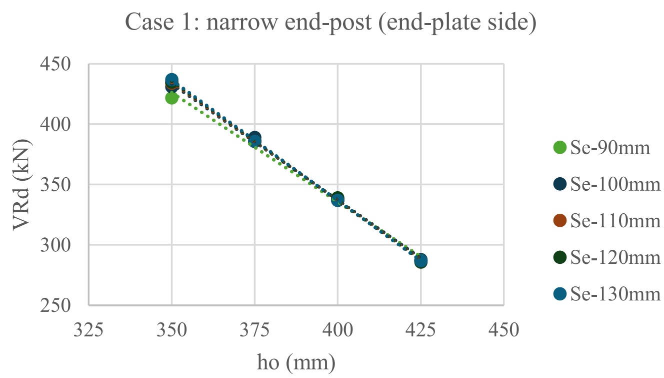

(a)

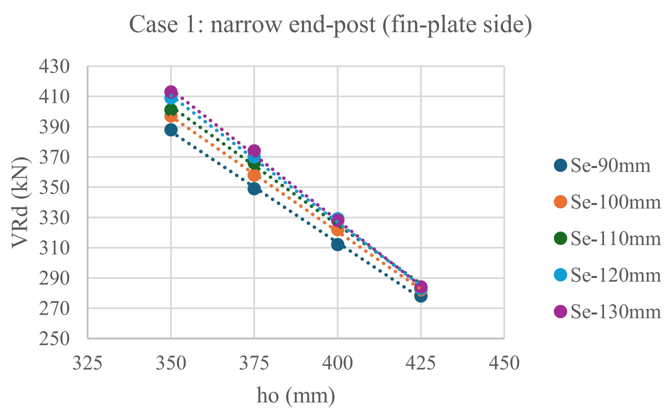

(b)

Fig. 14. End-post resistance with respect to the opening diameter (h_o) and the end-post width (s_e) for the two cases.

local buckling of the narrow end-post near the upper notch. As expected, the end-plate connections resulted in higher end-post resistances than the fin-plate connections by 3.8 % on average (see Table 7). The theoretical failure load is taken, as the minimum load in failure Modes 2 and 4 (see Appendix A).

4.6. Analysis of case 3 and 4 results with half infills

For the tests with half infills, the results are presented in Table 6. In case 3, the notch length c_n was 90 mm to 135 mm. Case 4 models had no notch ($c_n = 0$ mm).

When comparing the two connection types, the end-plate side failed at on average 1.2 % higher shear load than for the fin-plate side (see Table 7). The notch widths of 120 mm are outside the dimensional limits given in BS EN 1993-1-13 [9] for all cases. Fig. 15 shows the principal stress profile for the case of the smallest opening diameter and the longest notch. This shows that the effective loaded width acting on the infill plate is wider than s_e-c_n, but less than the simplified effective width of $b_{eff} = 0.25\ h_o$.

The fin-plate side models failed by buckling of the half infill plate due to the high compressive stresses in the upper Tee near the notch. In most of those cases, the initial buckling of the half infill plate was not critical, and a second failure followed in *Vierendeel* bending across the half opening. For the $h_o = 375$ mm fin-plate cases, the effect of the notch length c_n on the shear resistance was limited. Nearly all end-plate side models failed by *Vierendeel* bending, but failure by buckling of the half infill was also likely.

For the half infill cases without a notch (Case 4), a similar behaviour occurred, and the end-plate case failed at a load of only 1.2 % higher than the fin-plate case, which shows that the effect of the connection type on the stability of the infill plate is small. In all cases with half infills, yielding occurred early at the two corners of the semi-circular half infills, due to the high local stress concentrations caused by the *Vierendeel* bending moments at the reduced web section of the half-opening.

In order to compare the theory with the FE results, the effective width of the half infill with a notch as an equivalent strut is taken conservatively as:

$$\text{Notches within geometric limits}: b_{eff} = 0.25h_o \text{ for } c_n \leq s_e - 0.25h_o$$

$$\text{Long notches}: b_{eff} = s_e – c_n \text{ for } c_n > s_e - 0.25h_o$$

The analysis cases with $c_n = 120$ mm is outside the $c_n \leq 0.2$ h limit.

The comparison of the FE results with the theory (Mode 5) for the Cases 3 and 4 with half infill plates is presented in Table 6. It can be seen that the theory based on buckling of the infill plate is relatively conservative. However, the FE models assume a fully fixed interface between the infill plate and web, whereas in reality, partial fixity may exist because of the incomplete penetration of the welds to the infill plate. Also, the FE models allow for redistribution of forces between the Tees.

5. Conclusions

This paper extends the results of a test series on cellular beams, in order to update the Eurocode calculations for the design of end-post connections. Following the FE validation of the tests presented in [26], a parametric study was carried out to investigate the end-post behaviours of a wider range of end-post geometries. The study involved 160 end-post configurations, taking into consideration current practice, as well as the guidance provided by Eurocode 3 [9] and SCI P355 [7]. The presented theory and the FE analyses results showed that:

- The end-plate connection strengthened the end-post, allowing it to resist higher shear loads than the respective fin-plate side. Moreover, the cases with end-plates generally failed by *Vierendeel* bending at the first opening, which is justified by the fact that the stiffer end-plate connection provided greater stability and shear resistance to the end-post than the fin plate connection.
- Among the examined parameters, the results showed that the web opening diameter (h_o) was dominant in determining the end-post shear resistance. The end-post width, s_e, and the notch length, c_n, values had a smaller effect on the failure loads and modes.
- Two failure modes were observed in most of the cases with half infill plates. First, buckling of the half infill plate occurred at the upper part of the infill, which was followed by *Vierendeel* bending at the half opening. The half infill plates increased the failure load by 16 to 32 % on average for full depth end-posts and 19 to 44 % on average for notched end-posts.
- The proposed theory for buckling of the end-post is shown to be relatively conservative compared to the FE analyses but it should be noted that the FE models allow redistribution of shear forces between the Tees, which is not considered in the theory.
- The theory and FE results showed that the minimum width of the end-post can be reduced if the design resistances of the potential failure modes are calculated. For end-plate connections, end-post bending and horizontal shear are not likely to be critical failure modes and the minimum end-post width can be reduced to $0.2h_o$.
- The notched beams showed reduced end-post shear resistance, and the notches reduced the shear resistance by 5.5 to 11.5 % on average. For the notched beams with half infill plates the decrease was 2.5 to 7 % on average.

Table 5
Parametric study results compared to the theory in this paper for narrow end-posts with notched flanges.

Opening Diameter	End-post width, s_e (mm)	Notch length, c_n (mm)	Fin-plate connection			End-plate connection		
			FE failure load (kN)	Theory (kN)	FE/ Theory	FE failure load (kN)	Theory (kN)	FE/ Theory
350 mm (=0.62 h)	90	90	382	220	1.73	396	222	1.78
	100	90	382	243	1.57	394	246	1.60
	110	90	381	263	1.45	396	267	1.48
		105	379		1.44	394		1.47
	120	90	381	283	1.35	397	288	1.38
		105	379		1.34	395		1.37
		120	376		1.33	393		1.36
	130	90	382	302	1.26	396	312	1.27
		105	379		1.25	394		1.26
		120	378		1.25	392		1.25
375 mm (=0.67 h)	90	90	337	193	1.74	348	197	1.76
	100	90	335	211	1.59	348	218	1.59
	110	90	336	228	1.47	348	236	1.47
		105	333		1.46	346		1.46
	120	90	336	249	1.35	350	254	1.38
		105	334		1.34	345		1.36
		120	332		1.33	344		1.35
	130	90	339	261	1.30	351	275	1.27
		105	335		1.28	347		1.26
		120	332		1.27	344		1.25
400 mm (=0.71 h)	90	90	290	190	1.52	302	193	1.56
	100	90	290	211	1.37	301	211	1.42
	110	90	292	228	1.28	301	232	1.30
		105	289		1.27	297		1.28
	120	90	294	245	1.20	304	253	1.20
		105	290	240	1.21	300	245	1.22
		120	287	200	1.43	296	205	1.44
	130	90	297	261	1.14	309	269	1.15
		105	292	235	1.24	302	245	1.23
		120	288	195	1.47	298	205	1.45
425 mm (=0.76 h)	90	90	247	177	1.39	256	180	1.42
	100	90	248	196	1.26	258	200	1.29
	110	90	251	213	1.18	260	217	1.20
		105	246	195	1.26	256	205	1.25
	120	90	254	227	1.12	263	232	1.13
		105	248	215	1.15	257	220	1.17
		120	245	185	1.32	251	190	1.32
	130	90	259	235	1.10	270	245	1.10
		105	252	210	1.20	261	215	1.21
		120	246	180	1.36	254	185	1.37

Table 6
Parametric study results compared to the theory in this paper for end-posts with half infill plates. VB is the failure load due to *Vierendeel* bending at the first half-opening, indicating that end-post failure did not occur.

Opening Diameter	Notch length c_n (mm)	Fin-plate connection			End-plate connection		
		FE failure load (kN)	Theory (kN)	FE/Theory	FE failure load (kN)	Theory (kN)	FE/Theory
350 mm (=0.62 h)	0	491	320	1.53	499 VB	365	1.37
	90	476	304	1.56	479 VB	320	1.49
	105	466	304	1.53	476 VB	320	1.49
	120	457	290	1.57	463 VB	305	1.52
	135	427	238	1.79	455	250	1.82
375 mm (=0.67 h)	0	452	301	1.50	461 VB	331	1.39
	90	436	280	1.56	454 VB	301	1.51
	105	435	280	1.55	437 VB	301	1.45
	120	429	267	1.60	433 VB	266	1.63
	135	417	203	2.05	431 VB	218	1.98
400 mm (=0.71 h)	0	417	279	1.49	420 VB	305	1.38
	90	410	263	1.56	415 VB	279	1.49
	105	400	258	1.55	411 VB	273	1.50
	120	392	218	1.80	399 VB	232	1.72
	135	384	179	2.14	389 VB	190	2.05
425 mm (=0.76 h)	0	372	256	1.45	372 VB	279	1.33
	90	369	241	1.53	372 VB	256	1.45
	105	366	223	1.64	371 VB	237	1.56
	120	356	189	1.88	360 VB	200	1.80
	135	345	155	2.22	349	164	2.13

Table 7
Summary of the mean shear failure load values for each test, and comparison between FE and analytical predictions.

	Fin-plate connection			*End-plate connection*		
	FE failure load (kN)	Theory (kN)	*FE/ Theory*	*FE failure load (kN)*	*Theory (kN)*	*FE/ Theory*
Test 1	343	239	1.44	361	245	1.47
Test 2	314	235	1.34	326	241	1.35
Test 3	413	243	1.70	418	257	1.63
Test 4	433	289	1.50	438	320	1.37

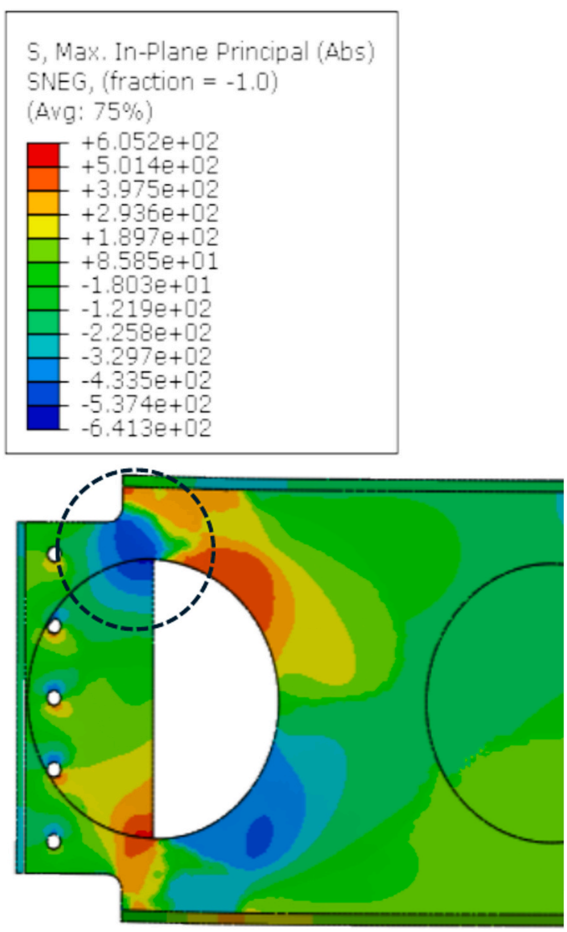

Fig. 15. Max. absolute in-plane principal stresses (MPa) when buckling of the half infill plate occurred in the model with the widest notch ($h_o = 350$ mm and $c_n = 135$ mm).

- The proposed theory for buckling of the half infill plate is shown to be relatively conservative to the FE analyses but it should be noted that the FE models assume full fixity between the infill plate and web, whereas in practice, this interface is affected by the partial strength of the welds to the infill plates.

The study also showed that the FE models allow for high plasticity and for redistribution of forces from the top to the bottom Tee, which could be included in the design models. The effect of end moments should be studied in future work.

CRediT authorship contribution statement

Georgios Psyrras: Writing – original draft, Software, Methodology, Investigation, Formal analysis, Data curation. **Konstantinos Daniel Tsavdaridis:** Writing – review & editing, Validation, Supervision, Project administration, Methodology, Investigation, Funding acquisition, Data curation, Conceptualization. **R. Mark Lawson:** Writing – review & editing, Validation, Supervision, Methodology, Investigation, Data curation, Conceptualization.

Declaration of competing interest

The authors declare that they have no known competing financial interests or personal relationships that could have appeared to influence the work reported in this paper.

Appendix A. Theoretical failure modes of end-posts

The modes of failure of the end-posts and their design expressions are presented in order to compare with the tests and with the parametric study of the end-post and notch geometry.

Mode 1: End–post horizontal shear

Narrow end-posts may fail in horizontal shear, which also leads to in plane bending, as shown in Fig. A.1. The horizontal shear force acting in the end-post is given by:

$$V_{ep} = V_{Ed}\frac{(s_e - e_b + 0.5h_o)}{h_{eff}} \tag{A.1}$$

where h_o is the opening diameter; e_b is the distance of line of bolts from the outer edge of the end-post; h_{eff} is the vertical distance between the centroid of the Tees ≈ 0.95 h; h is the depth of the section; s_e is the width of end-post; V_{Ed} is the design vertical shear force at the support.

The horizontal shear resistance of the end-post is limited by a shear strength of 0.577 f_y to BS EN 1993-1-1 [29]. For fin plate or angle connections, it may be assumed that a bolt hole occurs at the centre-line of the opening, which gives a horizontal shear resistance of:

$$V_{ep,Rd} = 0.577\ (s_e - \varnothing)\ t_w\, f_y \tag{A.2}$$

where t_w is the web thickness; f_y is the web yield strength; ∅ is the bolt hole diameter.

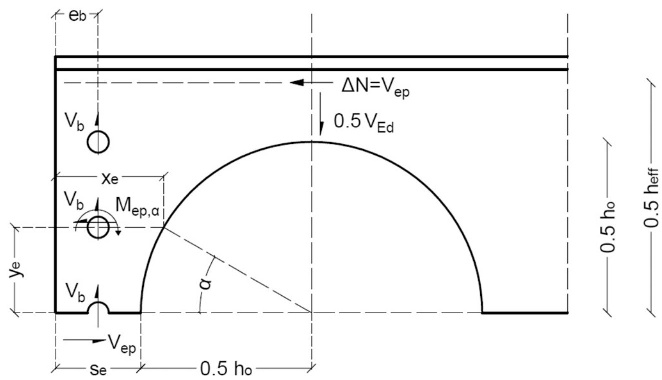

Fig. A.1. Illustration of horizontal shear and bending in a narrow end-post.

For end-plate connections, the horizontal shear resistance is increased by considering the shear force resisted by the end-plate acting as the flange of a Tee section. The horizontal shear resistance of the end-post including the contribution from the end-plate is given as a good approximation by:

$$V_{ep,Rd} = 0.577\ t_w\left(s_e f_y + t_{ep}\, f_{y,ep}\right) \tag{A.3}$$

where t_{ep} is the thickness of the end-plate; $f_{y,ep}$ is the yield strength of the end-plate.

Mode 2: Buckling of the end-post to BS EN1993-1-13

The design method for web buckling of end-posts is presented in BS EN1993-1-13 [9] This action in the end-post is shown in Fig. A.2, in which the compression force, $N_{ep,Ed}$, acting on the equivalent strut is taken as equal to the shear force in the top Tee and its effective width is taken as $b_{eff} = 0.5s_e$. For an end-post next to a circular opening, the effective length of the equivalent strut is taken as the diagonal distance over half of the end-post width and half of the opening depth. The equivalent strut slenderness is obtained by dividing the effective length by $t_w/12^{0.5}$, which gives an end-post slenderness ratio of:

$$\overline{\lambda}_{ep} = 1.75\ \frac{\left(s_e{}^2 + h_o{}^2\right)^{0.5}}{t_w\ \lambda_1} \leq \frac{2.45h_o}{t_w\ \lambda_1} \tag{A.4}$$

where $\lambda_1\ = 3.14\ \left(E/f_y\right)^{0.5}$.

The buckling resistance of the end-post is obtained from buckling curve ‘a’ to EN1993-1-1 [29], which is justified because the plate restraint to buckling is greater than that of the web considered as an equivalent strut.

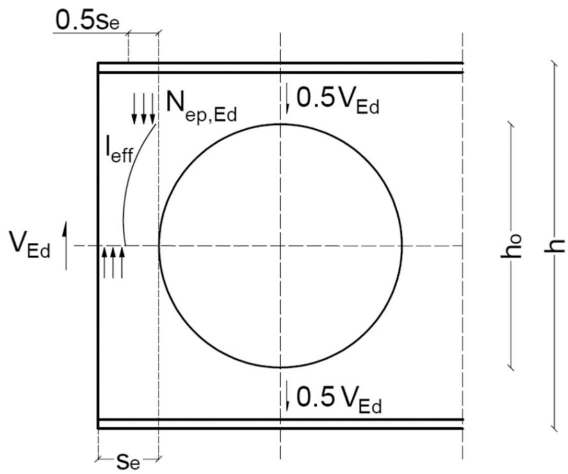

Fig. A.2. Illustration of strut buckling model for an end-post in BS EN 1993-1-13 [9].

For an end-post that is partly stabilised by an end-plate connection, the end-post slenderness is modified according to:

$$\overline{\lambda}_{ep} = 1.75\ \frac{\left((0.7s_e)^2 + {h_o}^2\right)^{0.5}}{t_w\ \lambda_1} \leq \frac{2.1h_o}{t_w\ \lambda_1} \tag{A.5}$$

For an end-post connected by a fin plate with partial loss of restraint by a notch to the compression flange, the end-post slenderness is modified according to:

$$\overline{\lambda}_{ep} = 1.75\ \frac{\left((1.2s_e)^2 + {h_o}^2\right)^{0.5}}{t_w\ \lambda_1} \leq \frac{2.7h_o}{t_w\ \lambda_1} \tag{A.6}$$

The buckling resistance of the end-post should exceed the compression force transferred from shear in the top Tee, which is given by:

$$N_{ep,b,Rd} = \chi_{ep}\ 0.5\ s_e\ t_w\, f_y \geq N_{ep,Ed} \tag{A.7}$$

Where χ_{ep} is the reduction factor due to buckling of the end-post using the non-dimensional slenderness in Eq. (A.5) and Eq. (A.6), and $N_{ep,Ed}$ is the compression force due to shear in the top Tee (= 0.5 V_{Ed} for a symmetric section).

For a symmetric section, the 0.5 factors on each side of this equation cancel to give the formula in BS EN 1993-1-13 [9]. This equivalent strut method is conservative because the lower part of the end-post acts in tension and can resist a higher tie force which leads to a re-distribution of shear forces between the Tees, which is not included in the design method.

Example. Fin plate connection (no notch) with $s_e = 100$ mm; $h_o = 400$ mm; $t_w = 9.0$ mm; $f_y = 355$ N/mm^2:

$$l_{eff} = 0.5\ \text{x}\ \left(100^2 + 400^2\right)^{0.5} = 206\ \text{mm}.$$

$$\lambda_{ep} = 3.46 \times 206/9.0 = 79$$

$$\overline{\lambda}_{ep} = 79/76 = 1.04$$

The end - post buckling resistance obtained using buckling curve 'a' is given by:

$$N_{b,Rd} = 0.63 \times 50 \times 9.0 \times 355 \times 10^{-3} = 100.6\ \text{kN}$$

For a symmetric section, the end shear force limited by end-post buckling is $V_{Ed} \leq 2N_{b,Rd} = 201$ kN.

Mode 3a: In-plane bending of narrow end-post to fin-plate or angle connection

A narrow end-post in a cellular beam may fail in in-plane bending due to the effect of the horizontal shear force, as shown in Fig. A.1. The critical distance y_e of the horizontal plane above the centre-line of the opening is when the in-plane bending resistance of the end-post is equal to the moment due to the horizontal shear force, V_{ep}.

For a fin plate connection with a line of bolts in vertical shear, the end-plate or fin plate should be connected to the web over a minimum length of 0.8 h, and it is assumed that the vertical shear force is distributed uniformly by the bolts in the connection.

The end-post horizontal shear force, V_{ep}, is given by Eq. (A.1), and the in-plane moment acting on any horizontal plane of the end-post and ignoring the restoring effect of the vertical shear force in the bolts over a distance y_e is given by:

$$M_{ep,\alpha} = V_{ep}\ y_e = V_{ep}\ 0.5\ h_o\ sin\alpha \tag{A.8}$$

where α is the angle from the centre of the opening to the height of the horizontal plane in the end-post.

The width of the end-post on the horizontal plane at an angle α is given by:

$$x_e = s_e + 0.5h_o(1 - cos\alpha) \tag{A.9}$$

The in-plane bending resistance of the end-post based on its plastic bending resistance is:

$$M_{ep,\alpha,Rd} = \frac{x_e{}^2}{4} t_w f_y \tag{A.10}$$

It is required that $M_{ep,\alpha} \leq M_{ep,Rd}$ and so the horizontal shear force in the end-post should be less than:

$$V_{ep} \leq \frac{(s_e + 0.5h_o(1 - cos\alpha))^2}{2\ h_o sin\alpha}\ t_w f_y \tag{A.11}$$

The critical in–plane section may be obtained by differentiating Eq. (A.11) with respect to α which reduces to a quadratic equation, with a solution given by:

$$cos\alpha = -\left(0.5 + \frac{s_e}{h_o}\right) + \left[\left(0.5 + \frac{s_e}{h_o}\right)^2 + 2\right]^{0.5} \tag{A.12}$$

For a typical narrow end-post with $s_e = 0.25h_o$, the critical angle is $\alpha = 32^o$ to the horizontal and $x_e \approx 1.3\, s_e$.

The critical height of the end-post for in-plane bending is given from Eq. (A.12) as approximately:

$$y_e \approx 0.55\ (s_e h_o)^{0.5} \tag{A.13}$$

The horizontal shear resistance for in-plane bending of the end-post with a fin-plate or double angle connection is obtained with reasonable accuracy from these equations as:

$$V_{ep,bending,Rd} = 0.77\left(\frac{s_e}{h_o}\right)^{0.5} s_e t_w f_y \tag{A.14}$$

The use of this method is given in the example below:

Example: $s_e = 100$ mm; $h_o = 400$ mm; $e_b = 35$ mm; $e_v = 60$ mm; $t_w = 9.0$ mm; $h = 600$ mm; $h_{eff} = 570$ mm; $f_y = 355$ N/mm^2:

The horizontal shear resistance in in-plane bending of the end-post is given in Eq. (A.14) as:

$$V_{ep,bending,Rd} = 0.77 \times 0.25^{0.5} \times 100 \times 9.0 \times 355 \times 10^{-3} = 123\ \text{kN}$$

The vertical shear force corresponding to this horizontal shear resistance in end-post bending is obtained from Eq. (A.1) as:

$$V_{Ed} = 123 \times \frac{570}{(100 + 200 - 35)} = 264\ \text{kN}$$

This shear force exceeds the end-post buckling resistance of 201 kN for a fin-plate connection (Mode 2) and shows that in-plane bending of the 100 mm wide end-post will not control.

Mode 3b: In-plane bending of narrow end-post with end-plate connection

For a narrow end-post in a cellular beam with an end-plate connection, the end-plate acts as the flange of a T-section together with the web of the end-post, and so it adds to the bending resistance on the horizontal plane. This also applies to a partial depth end plate connection in which the depth of the end-plate exceeds 0.8 h, as shown in Fig. A.3.

Generally, the plastic neutral axis of a T-section will be in or close to the flange (the end-plate in this case). In this case, the in-plane bending resistance of the end-post may be taken as:

$$M_{ep,\alpha,Rd} = 0.5x_e{}^2\ t_w\ f_y \tag{A.15}$$

where x_e is the width of the end-post at the critical section.

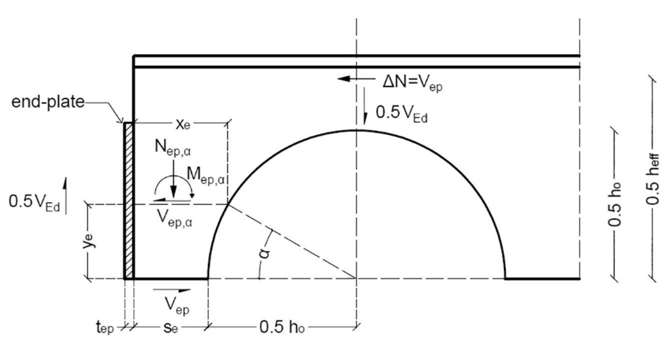

Fig. A.3. Moment acting on the horizontal plane of a narrow end-post with an end-plate connection.

Using the same approach as for fin plate connections, the horizontal shear resistance due to end-post bending is given by:

$$V_{ep,bending,Rd} = 1.54\left(\frac{s_e}{h_o}\right)^{0.5} s_e\ t_w\ f_y \tag{A.16}$$

It is apparent that this mode of failure will not occur for $s_e = 0.25h_o$. Therefore, minimum end-post width may be reduced to $s_e = 0.2h_o$ for end plate connections.

Mode 4: Local failure at a notch in the section due to compression and in-plane bending of the end-post

In a notched connection, part of the in-coming beam flange and web is cut away to connect the beam to a supporting beam. For a narrow end-post, the presence of the notch close to the opening reduces the resistance to *Vierendeel* bending on the notch side. The failure mode by plasticity and buckling at the narrow end-post at a notched connection is shown in Fig. A.4.

For use of this method, the maximum dimensions of the notches in a cellular beam are proposed as follows:

$$\text{Length of notch}: c_n \leq 0.2\ h, \text{but}\ c_n \leq s_e$$

$$\text{Depth of notch}: d_n \leq 0.1\ h$$

The equilibrium of forces and moments on a narrow end–post at the top Tee is shown in Fig. A.5. The minimum width of web is the radial distance between the corner of the notch and the edge of the opening, and for the top Tee, it is subject to a combination of axial compression and in-plane bending.

Fig. A.4. Buckling at narrow end post of notched beam.

The angle of the critical plane of the notch to the vertical is given by:

$$\theta_n = tan^{-1}\left(\frac{s_e - c_n + 0.5h_o}{0.5h - d_n}\right) \quad \text{(A.17)}$$

Where θ_n is the angle of the plane to the vertical from the centre of the opening.

For a notch with a corner radius, r_n, the inclined width, b_n, at the notch may be increased by approximately $0.4r_n$ and is given as follows:

$$b_n = \frac{0.5h - d_n}{cos\theta_n} - 0.5h_o + 0.4r_n \quad \text{(A.18)}$$

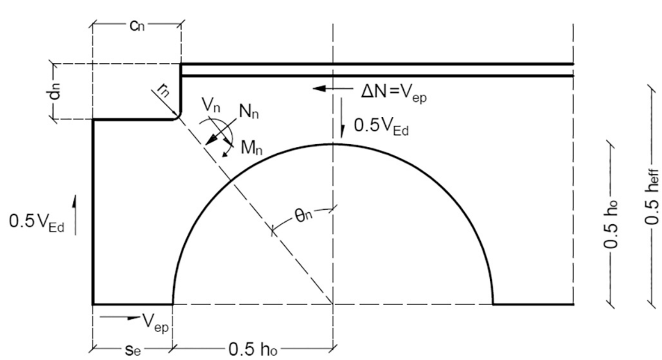

Fig. A.5. Forces on the notched end–post at the centre-line of the first opening.

The axial force acting normal to the inclined web at the notch is:

$$N_n = V_{ep}cos\theta_n + 0.5\ V_{Ed}\sin\theta_n \quad \text{(A.19)}$$

Inserting V_{ep} from Eq. (A.1) in Eq. (A.19) gives an axial force on the inclined web of:

$$N_n = 0.5V_{Ed}sin\theta_n\left[1 + \frac{(h_o + 2(s_e - e_b))}{h_{eff}}cot\theta_n\right] \quad \text{(A.20)}$$

At the first opening, it is reasonable to take h_{eff} = h-t_f, where t_f is the flange thickness.
Taking moments about the centre of b_n gives an in-plane moment at the notch as:

$$M_n = 0.5\ V_{ep}(h_o + b_n)\ cos\theta_n - 0.5\ V_{Ed}\ (c_n - e_b + 0.5b_n \sin\theta_n) \tag{A.21}$$

Inserting V_{ep} from Eq. (A.1) gives an in-plane moment of:

$$M_n = 0.25 V_{Ed}\left[\frac{(h_o + 2(s_e - e_b))}{h_{eff}}(h_o + b_n)cos\theta_n - 2(c_n - e_b) - b_n sin\theta_n\right] \tag{A.22}$$

For the top Tee, the reduced bending resistance of the web at the notch due to the combination of moment and axial force is given by:

$$M_{n,red,Rd} = M_{b,n,Rd}\left[1 - \left(\frac{N_n}{N_{b,n,Rd}}\right)^2\right] \tag{A.23}$$

The buckling resistance of the strut at the notch is: $N_{b,n,Rd} = \chi_n\ b_n\ t_w\ f_y$
where $\chi_n$is the reduction factor due to buckling of the web at the notch.
The plastic bending resistance of the narrow web at the notch is given by:

$$M_{n,Rd} = 0.25\ b_n^2\ t_w f_y \tag{A.24}$$

For compression acting on the narrow web at the notch, the end-post slenderness is dependent on the length of the unsupported web at the notch normal to the inclined width of the web. This may be approximated for design purposes as an effective buckling length of:

$$l_{eff} = c_n + d_n \tag{A.25}$$

The effective length is also dependent on the unsupported edge of the opening, which is given for design purposes as corresponding to a 40^o arc. This is given by a lower bound effective length of $l_{eff} \geq 0.35h_o$.

The buckling resistance of the narrow web is taken as its plastic resistance multiplied by χ_n, which is obtained from strut buckling curve ‘a’. Buckling does not occur for a web slenderness ratio of 0.4 taking account of the stabilising effect of the adjacent flange and web in comparison to an isolated strut, in which case $\chi_n = 1.0$. For combined bending and compression, this leads to a reduced bending resistance at the notch of:

$$M_{n,red,Rd} = \frac{b_n^2 t_w f_y}{4}\left[1 - \left(\frac{N_n}{b_n t_w \chi_n f_y}\right)^2\right] \tag{A.26}$$

For equilibrium, it is required that: $M_{n,red,\ Rd} \geq M_n$ and $N_{b,n,red,\ Rd} \geq N_n$.
Example for a notched beam with a fin plate connection: s_e = 100 mm; c_n = 90 mm (< s_e); d_n = 55 mm (< 0.1 h); r_n = 20 mm; h_o = 400 mm; h = 600 mm; h_{eff} = 570 mm; e_b = 35 mm; t_w = 9.0 mm; f_y = 355 N/mm^2:
Take the design shear force as V_{Ed} = 200 kN.

$$\theta_n = tan^{-1}\left(\frac{100 - 90 + 0.5 \times 400}{0.5 \times 600 - 55}\right) = 41^o \text{ to the vertical}$$

$$b_n = \frac{0.5 \times 600 - 55}{cos41} - 200 + 0.4 \times 20 = 132 \text{ mm}$$

$$l_{eff} = 90 + 55 = 145 \text{ mm} > 0.35 \times 400 = 140 \text{ mm}$$

The slenderness of the web at the notch is:

$$\lambda_{ep} = \frac{\ell_{eff}}{t_w/12^{0.5}} = \frac{145}{9.0} \times 3.46 = 56$$

For buckling curve ‘a’ the buckling resistance of the notched web as an equivalent strut is:

$$N_{b,n,Rd=}\ 0.82 \times 132 \times 9.0 \times 355 \times 10^{-3} = 346 \text{ kN}$$

Bending resistance of web at notch: $M_{n,Rd} = 0.25 \times 132^2 \times 9.0 \times 355 \times 10^{-6} = 13.9$ kNm

The compression force at the notch is: $N_n = 0.5 \times 200 \times 0.66\left[1 + \frac{(400+2\times65)}{570} \times 1.15\right] = 136$ kN

The horizontal shear force in the end-post is: $V_{ep} = 200 \times \frac{265}{570} = 93$ kN
The moment acting in the web at a notch is obtained from Eq. (A.21) is:

$$M_n = 0.5 \times 93 \text{ x } (400 + 132) \text{ x } 0.75 \times 10^{-3} - 0.5 \times 200 \text{ x } (55 + 0.5 \times 132 \times 0.66) \text{ x } 10^{-3} = 18.5\text{–}9.8 = 8.7 \text{ kNm}$$

The reduced bending resistance of the web at the notch when subject to compression is:

$$M_{n,red,Rd} = 13.9 \times \left[1 - \left(\frac{146}{346}\right)^2\right] = 11.4 \text{ kNm} > 8.7 \text{ kNm}$$

This shows that the resistance of the end-post at the notch is satisfied for a design shear force of V_{Ed} = 200 kN.

Mode 5: Design of half infill plates to form an end-post in a cellular beam

A half infill plate may be used to satisfy the minimum width of the end-post and to provide the necessary shear resistance in the case of a notched beam, as shown in Fig. A.6. For use of half infill plate, the minimum width of the end post is $s_e \geq 0.5h_o$ and if this is not satisfied, a full infill plate should be used.

The limits on the notch dimensions for use of half infill plates to cellular beams may be taken as the same as for as for a plain beam but with the additional requirement that $c_n \leq 0.5s_e$, where s_e is the width of the end-post including the half infill. A further limit is that $c_n \leq 0.2$ h to avoid local instability of the top flange. An isolated half infill plate is designed as an equivalent strut to transfer the compression force from the top Tee. The effective width of the half infill plate is taken as $b_{eff} = 0.25h_o$.

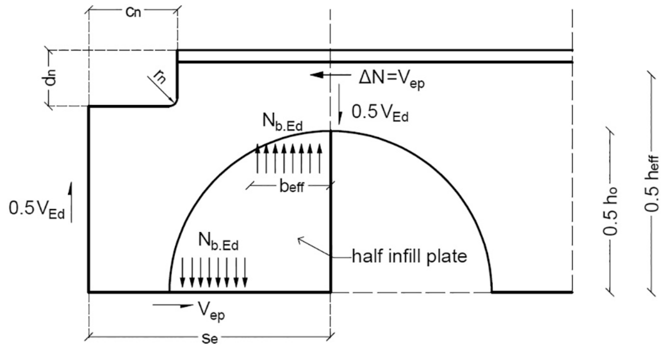

Fig. A.6. Forces in end-post formed by a half infill plate.

The equivalent slenderness ratio of the infill plate is adapted from Eq. (A.4) and is therefore:

$$\bar{\lambda}_i = \frac{1.75\left((0.5h_o)^2 + h_o^{\,2}\right)^{0.5}}{t_i\lambda_1} = \frac{1.95h_o}{t_i\lambda_1} \tag{A.27}$$

where t_i is the infill plate thickness ($\leq t_w$); $f_{y,i}$ is the yield strength of infill plate ($\leq f_y$)

The buckling resistance of the infill plate should satisfy:

$$N_{i,Rd} = \chi_i\, b_{eff}\, t_i\, f_{y,i} \geq N_{b,Ed} \tag{A.28}$$

where χ_i is the reduction factor due to buckling of the infill plate; $N_{b,Ed}$ is the compression force transferred from the top Tee ($= 0.5V_{Ed}$ for a symmetric section).

Example for half infill plate: $s_e = 200$ mm; $h_o = 400$ mm; $t_i = 9.0$ mm; $f_y = 355$ N/mm^2:

$$l_{eff} = 0.5 \text{ x } \left(200^2 + 400^2\right)^{0.5} = 234 \text{ mm}$$

$$\lambda_{ep} = 3.46 \times 234/9.0 = 90$$

$$\bar{\lambda}_{ep} = 90/76 = 1.18$$

The buckling resistance of the half infill plate is:

$$N_{b,Rd} = 0.54 \times 100 \times 9.0 \times 355 \times 10^{-3} = 172.5 \text{ kN}$$

For a symmetric section, it follows that the end shear force, $V_{Ed} \leq 2N_{b,Rd} = 345$ kN when limited by buckling of the half infill plate.

Data availability

No data was used for the research described in the article.

References

[1] K.F. Chung, T.C.H. Liu, A.C.H. Ko, Investigation on Vierendeel mechanism in steel beams with circular web openings, J. Constr. Steel Res. 57 (5) (2001), https://doi.org/10.1016/S0143-974X(00)00035-3.
[2] K.D. Tsavdaridis, Structural Performance of Perforated Steel Beams with Novel Web Openings and with Partial Concrete Encasement, Doctoral thesis, City University London, 2010.
[3] K.D. Tsavdaridis, C. D'Mello, Web buckling study of the behaviour and strength of perforated steel beams with different novel web opening shapes, J. Constr. Steel Res. 67 (10) (2011), https://doi.org/10.1016/j.jcsr.2011.04.004.
[4] K.D. Tsavdaridis, C. D'Mello, Vierendeel bending study of perforated steel beams with various novel web opening shapes through nonlinear finite-element analyses, J. Struct. Eng. 138 (10) (2012), https://doi.org/10.1061/(asce)st.1943-541x.0000562.
[5] K.D. Tsavdaridis, C. D'Mello, Optimisation of novel elliptically-based web opening shapes of perforated steel beams, J. Constr. Steel Res. 76 (2012) 39–53.
[6] J.K. Ward, Design of Composite and Non-composite Cellular Beams, SCI Publication, 1990, p. 100.
[7] R.M. Lawson, S.J. Hicks, Design of Composite Beams with Large Web Openings, 2011. SCI P355.
[8] S.S. Fares, J. Coulson, D.W. Dinehart, AISC 31 Design Guide: Castellated and Cellular Beam Design, American Institute of Steel Construction, 2016.
[9] British Standards Institution, Eurocode 3: Design of Steel Structures - Part 1–13: Beams with Large Web Openings, 2024. BS EN 1993-1-13:2024.
[10] M.D. Altifillisch, B.R. Cooke, A.A. Toprac, An investigation of open web expanded beams, Weld. Res. 22 (2) (1957).
[11] R.G. Redwood, J.O. McCutcheon, Beam tests with unreinforced web openings, J. Struct. Div. 94 (1) (1968) 1–17.
[12] R.G. Redwood, Design of Beams with Web Holes, Canadian Steel Industries Construction Council, 1973.

[13] K.F. Chung, C.H. Liu, A.C.H. Ko, Steel beams with large web openings of various shapes and sizes: an empirical design method using a generalised moment-shear interaction curve, J. Constr. Steel Res. 59 (9) (2003), https://doi.org/10.1016/S0143-974X(03)00029-4.
[14] V.V. Degtyarev, K.D. Tsavdaridis, Buckling and ultimate load prediction models for perforated steel beams using machine learning, J. Build. Eng. 51 (2022) 104316.
[15] V.V. Degtyarev, S.J. Hicks, F.P.V. Ferreira, K.D. Tsavdaridis, Design resistance assessment for the resistance of laterally restrained cellular steel beams, J. Constr. Steel Res. 226 (2025) 109254.
[16] F. Erdal, M.P. Saka, Ultimate load carrying capacity of optimally designed steel cellular beams, J. Constr. Steel Res. 80 (2013) 355–368. Available at: https://doi.org/10.1016/J.JCSR.2012.10.007.
[17] L.F. Grilo, et al., Design procedure for the web-post buckling of steel cellular beams, J. Constr. Steel Res. 148 (2018), https://doi.org/10.1016/j.jcsr.2018.06.020.
[18] R. Shamass, F.P.V. Ferreira, V. Limbachiya, L.F.P. Santos, K.D. Tsavdaridis, Web-post buckling prediction resistance of steel beams with elliptically-based web openings using artificial neural networks (ANN), Thin-Walled Struct. 180 (2022) 109959.
[19] F.P.V. Ferreira, R. Shamass, L.F.P. Santos, V. Limbachiya, K.D. Tsavdaridis, EC3 design of web-post buckling resistance for perforated steel beams with elliptically-based web openings, Thin-Walled Struct. 175 (2022) 109196.
[20] F.P.V. Ferreira, R. Shamass, L.F.P. Santos, K.D. Tsavdaridis, V. Limbachiya, Web-post buckling resistance calculation of perforated high-strength steel beams with elliptically-based web openings for EC3, Structures 55 (2023) 245–262.
[21] M. Rabi, Y.S. Jweihan, I. Abarkan, F.P.V. Ferreira, R. Shamass, V. Limbachiya, K. D. Tsavdaridis, V. Santos, Machine learning-driven web-post buckling resistance prediction for high-strength steel beams with elliptically-based web openings, Results Eng. 21 (2024) 101749.
[22] E.V. Santos, F.P.V. Ferreira, K.D. Tsavdaridis, C.H. Martins, R.M. Lawson, Web-post buckling of steel-concrete composite beam with elliptically-based web openings, J. Constr. Steel Res. 229 (2025) 109483.
[23] B.M. Zeytinci, M. Sahin, M.A. Güler, K.D. Tsavdaridis, A practical design formulation for perforated beams with openings strengthened with ring type stiffeners subject to Vierendeel actions, J. Build. Eng. 43 (2021) 102915.
[24] R.M. Lawson, et al., Design of composite asymmetric cellular beams and beams with large web openings, J. Constr. Steel Res. 62 (6) (2006), https://doi.org/10.1016/j.jcsr.2005.09.012.
[25] The Steel Construction Institute, Joints in steel construction: simple joints to Eurocode 3, SCI P358 (2017).
[26] K.D. Tsavdaridis, B. McKinley, D.A. Corfar, R.M. Lawson, Cellular beam end-posts with two connection types, end notches and infill plates, J. Constr. Steel Res. 215 (2024) 108547, https://doi.org/10.1016/J.JCSR.2024.108547.
[27] Dassault Systèmes, Abaqus/CAE 2020, Available at: https://www.3ds.com/products-services/simulia/products/abaqus/, 2020.
[28] Dassault Systèmes, Abaqus 2020 Reference Library, Available at: https://help.3ds.com/2020x/, 2020.
[29] British Standards Institution, Eurocode 3: Design of Steel Structures - Part 1–1: General Rules and Rules for Buildings, 2005. BS EN 1993-1-1:2006.